

Fidelity susceptibility as a diagnostic of the commensurate-incommensurate transition: A revisit of the programmable Rydberg chain

Xue-Jia Yu,^{1,*} Sheng Yang,^{2,*} Jing-Bo Xu,^{2,†} and Limei Xu^{1,3,4,‡}

¹*International Center for Quantum Materials, School of Physics, Peking University, Beijing 100871, China*

²*Zhejiang Institute of Modern Physics and Department of Physics, Zhejiang University, Hangzhou 310027, China*

³*Collaborative Innovation Center of Quantum Matter, Beijing, China*

⁴*Interdisciplinary Institute of Light-Element Quantum Materials and Research Center for Light-Element Advanced Materials, Peking University, Beijing, China*

(Dated: July 19, 2022)

In recent years, programmable Rydberg atom arrays have been widely used to simulate new quantum phases and phase transitions, generating great interest among theorists and experimentalists. Based on the large-scale density matrix renormalization group method, the ground-state phase diagram of one-dimensional Rydberg chains is investigated with fidelity susceptibility as an efficient diagnostic method. We find that the competition between Rydberg blockade and external detuning produces unconventional phases and phase transitions. As the Rydberg blockade radius increases, the phase transition between disordered and period-3 density-wave ordered phases changes from the standard three-state Potts to the unconventional chiral universality class. As the radius increases further, a very narrow intermediate floating phase begins to appear. This result provides a concise physical picture to illustrate the numerical results. Compared with previous studies, this work provides more evidence for non-conformal quantum phase transitions in programmable quantum simulators from the perspective of quantum information, showing that fidelity susceptibility can be used to study commensurate-incommensurate phase transitions.

I. INTRODUCTION

Mastering exotic phases and correlated phase transitions in quantum many-body systems is one of the core issues in condensed matter physics [1, 2]. Unlike phase transitions driven by thermal fluctuations, quantum systems driven only by quantum fluctuations can undergo quantum phase transitions at absolute zero temperature. By tuning non-thermal parameters such as doping in the parent compound of high- T_c superconductors [3], magnetic field in quantum Hall samples [4], pressure in quantum magnetic systems [5, 6], and disorder in a conductor near its metal-insulator transition [7], the ground state of a quantum system can change fundamentally, including scaling behaviors and universality categories. Unconventional quantum phase transitions have attracted great interest in the past few decades [8–11] and have raised new questions both theoretically and experimentally, especially the absolute necessity to consider quantum effects [1].

The concept of universality classes plays a crucial role in continuous phase transitions and quantum criticality [12]. Quantum many-body systems with nearest-neighbor interactions, such as the quantum transverse-field Ising model, the Heisenberg model, and the Hubbard model, are crucial for understanding quantum phase transitions [1]. By constructing a simplified lattice model, the same low-energy physics can be studied in

terms of the concept of universality, even if we use different microscopic lattice Hamiltonians. Furthermore, many quantum critical points are marked by the emergence of scale invariance or conformal symmetry, and the corresponding universality class can be described by conformal field theories (CFTs) with a dynamical critical exponent $z = 1$ [12–14].

Recently, neutral Rydberg atoms trapped in optical tweezers with programmable van der Waals type interactions [15–18] provide a promising tunable platform for observing various quantum phenomena, such as the gapped \mathbb{Z}_2 quantum spin liquid [19–26], quantum phase transitions between different density-wave-ordered and disordered phases [27–33], quantum Kibble-Zurek mechanism [15, 34, 35], and unexpected quantum many-body scars [36, 37]. However, for long-range quantum many-body systems, it remains challenging to fully understand their critical behaviors, either through theoretical methods or numerical simulations. As a prototype example, quantum phase transitions in the Rydberg chain are even more subtle. The Kibble-Zurek (KZ) experiments [15, 34, 35] dynamically probe quantum phase transitions between an incommensurate (IC) disordered phase and a commensurate (C) ordered phase with period $p = 3, 4, \dots$, sparking interest in the C-IC transition first proposed in the context of adsorbed monolayers in 1980s and 1990s [38–41]. The C-IC transition with $p \geq 5$ emerges through an intermediate gapless floating phase (Luttinger liquid) with a central charge $c = 1$, characterized by incommensurate correlations and wave vector q [42–46]. On the one hand, disorder-to-floating transitions belong to the Kosterlitz-Thouless (KT) universality class with exponentially diverged correlation lengths. On the other hand, the transition from

* The first two authors contributed equally.

† xujb@zju.edu.cn

‡ limei.xu@pku.edu.cn

the floating phase to the commensurate ordered phase is the Pokrovsky-Talapov (PT) transition. However, for $p = 3, 4$, as suggested by Huse and Fisher [39–41], if the chiral perturbations are correlated, the C-IC transition may still be direct without intermediate phase, but fall into the category of chiral universality class, which cannot be described by CFTs. This question was raised again by Fendley et al. [47, 48]. It is also related to the recent Rydberg atom experiment in the context of one-dimensional quantum models of constraint bosons. Chepiga et al. [45, 49] provide strong numerical evidence that intermediate floating phases can occur sufficiently far from the integrable Potts point, confirmed by extrapolation of correlation lengths and incommensurate wave vectors. However, Samajdar et al. [50, 51] claim that there is a continuous chiral transition between the disordered phase and the period-3 ordered phase, without an intermediate phase. Notably, with the newly developed tensor network method [45], the system size of previous calculations reaches up to 9000 sites, and the scaling properties of the wave vector and the correlation lengths around the critical points can be precisely obtained. It will be interesting to see if there is any other physical quantity that can efficiently identify possible unconventional phases or phase transitions with relatively small system sizes. Therefore, it is worth revisiting this period-3 ordered-to-disordered phase transition from a different perspective.

In this work, we use the concept of fidelity sensitivity borrowed from quantum information theory [52, 53] to study the period-3 ordered-to-disordered phase transition realized in programmable Rydberg chains, which may provides a new perspective on the C-IC transition. As a purely geometric measure of quantum states, fidelity susceptibility is believed to be effective in characterizing sudden changes in ground-state structure associated with quantum phase transitions, and over the past few years this concept has been established as one of the powerful diagnostics methods for quantum phase transitions without prior knowledge of order parameters or associated symmetry-breaking patterns. To date, fidelity susceptibility has been applied to detect various quantum critical points, such as conventional symmetry-breaking quantum critical points (e.g. Ising critical point) [54, 55], topological phase transitions [56], Anderson transitions [57, 58], deconfined quantum criticality [59], and even non-Hermitian critical points [60–62]. In this work, we will show that this concept could also be an attractive tool for studying challenging C-IC problems. Specifically, the fidelity susceptibility of quantum phase transitions can be experimentally detected by neutron scattering or the angle-resolved photoemission spectroscopy techniques [52, 63].

The rest of this paper is organized as follows: Sec. II contains a brief introduction to the lattice model of the Rydberg atom chain and the numerical method adopted. A brief review of the fidelity susceptibility and its scaling behavior is also given therein. A standard finite-size scal-

ing analysis is applied to study the transition from the period-2 ordered phase to the disordered phase which belongs to the Ising universality in Sec. III. The intermediate floating phase or exotic chiral phase transition between the disordered phase and the period-3 ordered phase is then explored with the same approach, and a brief explanation of the numerical results is provided in Sec. IV. Finally, we give a conclusion in Sec. V.

II. MODEL AND METHODS

In this work, we study the Hamiltonian of interacting Rydberg atoms arranged in a one-dimensional chain of length L with open boundary conditions [31],

$$H_{\text{Ryd}} = \sum_{i=1}^L \left[\frac{\Omega}{2} (|r\rangle_i \langle g| + |g\rangle_i \langle r|) - \delta |r\rangle_i \langle r| \right] + \sum_{i < j} V(|i-j|) |r\rangle_i \langle r| \otimes |r\rangle_j \langle r|. \quad (1)$$

Here, i represents the discrete sites of the Rydberg lattice (with lattice constant a). $|g\rangle_i$ and $|r\rangle_i$ denote the internal atomic ground state and an excited Rydberg state of the i th atom, respectively. The Rabi frequency Ω and detuning δ characterize a coherent laser driving field. $V(|i-j|) = C_6/|i-j|^6$ is the strength of the van der Waals interaction of atoms excited to the Rydberg state $|r\rangle$. The long-range interactions here can also be equivalently parametrized by the Rydberg blockade radius R_b , which is defined by $V(R_b/a) \equiv \Omega$ [31], where interactions are so strong that the Rydberg excitation of one atom suppresses the excitation of other atoms. This effect is called the Rydberg blockade mechanism. Notably, the model Hamiltonian H_{Ryd} can be mapped to the hard-core boson model by identifying $|g\rangle$ and $|r\rangle$ as the empty state and occupied state, respectively [47, 48]. For simplicity, Ω and a are set to energy and length units in our actual numerical simulations.

The ground state of the Rydberg Hamiltonian, $|\phi\rangle$, depends sensitively on the detuning δ/Ω and the blockade radius R_b/a , which govern the density of Rydberg excitation $n \equiv \langle \phi | (\sum_i |r\rangle_i \langle r| / L) | \phi \rangle$. At large negative δ/Ω , it is favorable for most atoms to be in the electronic ground state $|g\rangle$, which corresponds to the disordered phase. Whereas for large positive values of δ/Ω , the Rydberg excitation density n increases, and due to the Rydberg blockade mechanism, complex density-wave ordered phases with different spatial symmetries will be established depending on R_b/a , called ‘‘Rydberg crystal’’ phases [Fig. 1.]

Since there is no exact analytical solution for the general Rydberg Hamiltonian H_{Ryd} , we employ a large-scale finite-size density matrix renormalization group (DMRG) method [64, 65] in the representation of matrix product states (MPS) [66], which is one of the most powerful numerical methods for 1D strongly correlated many-body

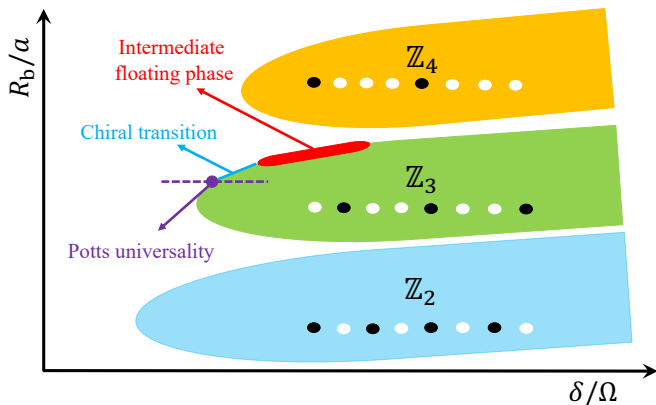


FIG. 1. Schematic ground-state phase diagram of the Rydberg chain with respect to Rydberg blockade radius R_b/a and detuning δ/Ω . \mathbb{Z}_n ($n = 2, 3, 4$) represents the \mathbb{Z}_n symmetry-breaking phase. The purple dot refers to the phase transition belonging to the three-state Potts universality class. The blue line represents the non-conformal chiral phase transition. The red region indicates the potential intermediate floating phase.

problems today for solving the ground state of H_{Ryd} . More specifically, to reduce the computational requirement due to the long-range interaction term $V(r)$, we employ a truncation strategy similar to that used in Ref. [50]. This leads to the so-called U-V model (see the Eq. (17) therein). In real simulations, however, we preserve interactions at most fourth-nearest neighbors by forcing $V(r) = 0$ when $r > 4$. Compared to the U-V model, the Hamiltonian with interaction truncation used here is more relevant to actual experiment and can more faithfully simulate the effective physics of the period-3 ordered-to-disordered phase transition in the Rydberg chain.

We note that the disordered to period- p ordered-to-disorder phase transitions of the model will be studied together with a fixed R_b line, so the Hamiltonian therefore can be viewed as a function of detuning. Fidelity susceptibility can then be calculated as [67, 68]

$$\chi_F(\delta) = \lim_{d\delta \rightarrow 0} \frac{2[1 - |\langle \phi(\delta) | \phi(\delta + d\delta) \rangle|]}{(d\delta)^2}, \quad (2)$$

where $|\phi(\delta)\rangle$ is the ground state of $H_{\text{Ryd}}(\delta)$. The fidelity, $F(\delta, d\delta) = |\langle \phi(\delta) | \phi(\delta + d\delta) \rangle|$, is defined as the overlap amplitude of two nearby quantum states in the parameter space. The fidelity is expected to drop sharply at quantum critical point, reflecting a sudden change in the ground-state structure. Therefore, the susceptibility $\chi_F(\delta)$, which is the dominant quadratic term with respect to $d\delta$ in the fidelity expansion, can faithfully diagnose general quantum phase transitions. Specifically, fidelity susceptibility has been successfully used to study other types of quantum phase transitions, including conventional phase transitions [54, 55] and unconventional quantum phase transitions [56, 59]. We emphasize that the application of this method does not rely on any prior knowledge of the underlying order parameters.

For continuous quantum phase transitions, it has been established in the literature that the fidelity susceptibility obeys certain finite-size scaling laws near quantum critical points. This paves the way for extracting quantum relevant key indices about critical exponents. In particular, the fidelity susceptibility exhibits a universal dependence on the control parameter described by the functional form [52, 53, 69]

$$\chi_F(\delta, L) = L^{2/\nu} \mathcal{F}_F[L^{1/\nu}(\delta - \delta_c)], \quad (3)$$

where ν is the correlation length exponent and \mathcal{F}_F is an unknown scaling function. Furthermore, for finite-size systems, the fidelity susceptibility at the pseudocritical point δ_m also shows a power law with respect to the chain length L ,

$$\chi_F(\delta \rightarrow \delta_m, L) \propto L^{2/\nu}. \quad (4)$$

We note that some sub-leading terms usually on the right-hand side of this relation could be ignored if the system size is large enough. Based on the above two scaling forms, it is easy to obtain the value of ν for the quantum phase transition we are interested in here and to determine whether it is continuous or not.

To further reveal the nature of the chiral or non-chiral phase transitions, we also calculate the energy gap Δ , which is defined as the energy difference between the first excited state and the ground state of H_{Ryd} , to obtain the dynamical critical exponent z . For continuous phase transitions, it is expected that the energy gap will disappear with $\Delta \sim |\delta - \delta_c|^{z\nu}$ as δ approaches δ_c [1]. Combined with the divergence of the correlation length following the form, $\xi \sim |\delta - \delta_c|^{-\nu}$, we obtain the scaling relation, $\Delta \sim \xi^{-z}$. Since the correlation length of the critical point of a finite system can be characterized by the lattice length L , the finite-size scaling law, $\Delta(\delta \rightarrow \delta_m, L) \propto L^{-z}$, can be finally derived. In addition, the energy gap also exhibits a similar functional form to the fidelity susceptibility [50]

$$\Delta(\delta, L) = L^{-z} \mathcal{F}_\Delta[L^{1/\nu}(\delta - \delta_c)], \quad (5)$$

where \mathcal{F}_Δ is another scaling function associated with Δ . We note that the dynamical critical exponent z equals to 1 for conformal universality classes.

III. WARM-UP: ISING UNIVERSALITY CLASS

In the following, based on the scaling laws listed above, we first test the fidelity susceptibility and energy gap approach to determine the dynamical critical exponent z and the correlation length exponent ν for the case of (1 + 1)D Ising universality class.

We first consider the period-2 ordered-to-disordered transition, which belongs to the (1 + 1)D Ising universality class [1] and has been well studied. This allows us to test the feasibility of the fidelity and energy gap approach to determine the critical exponents ν and z .

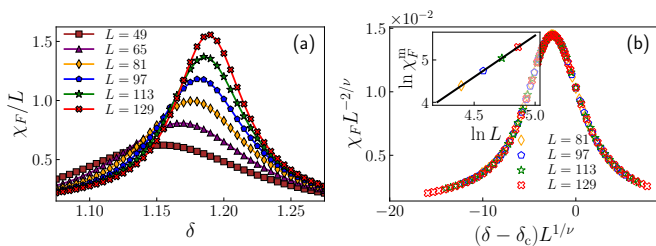


FIG. 2. Finite-size scaling analysis of the fidelity susceptibility for the period-2 ordered-to-disordered transition with a fixed blockade radius $R_b = 1.6$. (a) The fidelity susceptibility per site shows a sharp peak near the transition point. (b) Data collapse of the rescaled fidelity susceptibility and detuning with $\nu = 1.019$ and $\delta_c = 1.210$ for various system sizes. The inset shows the log-log plot of the fidelity susceptibility against the system size at the pseudocritical point, and the correlation length critical exponent $\nu = 1.019$ can be inferred from the slope of the fitted straight line.

To avoid defects induced by edge excitation and thus stabilize the ordered phase in the bulk, we consider system sizes $L = 2n + 1$, ranging from $L = 49$ to 129 for the period-2 ordered-to-disordered transition in our DMRG simulations with open boundary conditions. The MPS bond dimension is set to 300; when calculating the ground state and the first excited state, a good convergence to the true energy eigenstates is guaranteed by requiring the relative energy error to be smaller than 10^{-10} and 10^{-8} , respectively. For the fidelity susceptibility, we set a stricter convergence criterion with a relative energy error lower than 10^{-12} , and the detuning step is chosen as $d\delta = 10^{-3}$.

Fig. 2(a) shows the fidelity susceptibility per site χ_F/L as a function of detuning δ , with a fixed blockade radius $R_b = 1.6$. χ_F/L exhibits a sharp peak near the critical point and the divergence behavior can be described by conventional scaling laws, as expected from Eqs. (3) and (4). To extract the value of ν , we calculate more points around the peak for each system size to obtain fidelity susceptibility χ_F^m at the finite-size pseudocritical points δ_m . The inset of the Fig. 2(b) exhibits a linear fit to the DMRG data of the largest four system sizes using the least square method, consistent with a linear correlation of the logarithm of χ_F^m to $\ln L$ based on Eq. (4). An accurate estimation of the critical exponent $\nu = 1.019$ can then be easily acquired from the slope of the fitted line. On the other hand, the presence of the scaling function \mathcal{F}_F (see Eq. (3)) usually provides an independent verification of the correctness of the critical exponents. Using the value of ν obtained from the log-log plot and a fine tuning of the critical point δ_c (considered here as a tunable variable), we use the rescaled variables $\chi_F L^{-2/\nu}$ and $(\delta - \delta_c) L^{1/\nu}$ for various system sizes L . By implementing good data collapse, as shown in Fig. 2(b), the critical point can eventually be located at $\delta_c = 1.210(2)$, and the associated uncertainty is determined from visible imperfection observed in the process.

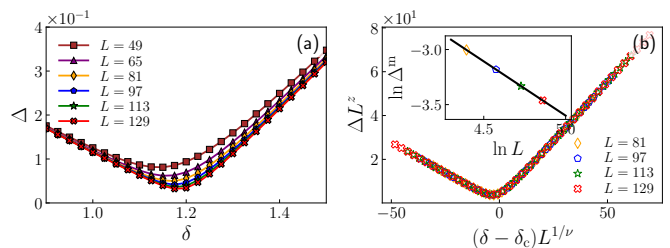


FIG. 3. Finite-size scaling analysis of the energy gap for the period-2 ordered-to-disordered transition with a fixed blockade radius $R_b = 1.6$. (a) The energy gap develops a deep valley near the transition point. (b) Data collapse of the rescaled energy gap and detuning with $z = 0.9847$, $\nu = 1.019$, and $\delta_c = 1.210$ for the largest four system sizes. The inset displays the log-log plot of the energy gap Δ^m versus the system size L at the pseudocritical point δ_m , and the fitted straight line has a slope whose absolute value equals to the exponent z .

We now obtain δ_c and ν via a standard finite-size scaling analysis of fidelity susceptibility. However, a single critical exponent, such as ν , is not sufficient to determine the universality class to which a quantum phase transition belongs. Therefore, we also acquire the dynamical critical exponent z from a similar scaling analysis of the energy gap Δ . The two-fold degeneracy of the ground state in the period-2 ordered phase is split here due to the addition of an extra site on the right edge, and the energy gap should show a deep valley near the transition point (see Fig. 3(a)) rather than vanishing to zero by entering into the ordered phase. Following a similar logic followed in the fidelity susceptibility analysis, we first estimate the exponent z from the log-log plot of the gap Δ^m at the pseudocritical point δ_m versus system size L . It is evident from the inset of Fig. 3(b) that the logarithm of Δ^m shows a perfect linear dependence on $\ln L$, the absolute value of whose slope should equal to z . By exploiting least square method, we end up with an estimation of $z = 0.9847$, which is very close to 1. Finally, we also use the scaling function \mathcal{F}_Δ to confirm the accuracy of the z estimation. By inserting $z = 0.9847$ obtained from the log-log plot as well as $\nu = 1.019$ and $\delta_c = 1.210$ inferred from the fidelity approach into Eq. (5), good collapse of curves [Fig. 3(a)] without any free parameters can be established [Fig. 3(b)]. Note that the values of ν and δ_c used in this collapse are obtained independently from the fidelity method, so such a full collapse also shows that the fidelity and energy gap methods agree with each other.

Together with the value obtained so far for the critical exponents $\nu = 1.019$ and $z = 0.9847$, we can now see within reasonable numerical precision that this result agrees with the well-known results in (1+1)D Ising universality class for $\nu = 1$ and $z = 1$. We attribute the small difference to a potential finite-size effect; considering larger system sizes can reduce this bias in a controllable manner. Thus, our results strongly demonstrate that the transition between the disordered phase and

the period-2 ordered phase realized in Rydberg chains belongs to the (1+1)D Ising universality class. In Appendix A, we also provide a finite-size scaling analysis of the same phase transition but with a blockade radius $R_b = 1.4$, which leads to the same conclusion.

IV. NON-CONFORMAL CRITICAL POINT: CHIRAL UNIVERSALITY CLASS

As can see from Sec. III, the combination of fidelity susceptibility and energy-gap methods provide a very powerful and self-consistent way to determine critical exponents and the universality class of quantum phase transitions. We therefore use this approach and follow the same logic used above in analyzing the period-2 ordered-to-disorder transition, to investigate the more complicated period-3 ordered-to-disordered transition hosted by the programmable Rydberg chain.

As a manifestation of the C-IC problem in 1D quantum systems, the disordered-to-period-3 ordered transition realized in the Rydberg chain is an ideal place to explore the nature of C-IC transitions, though challenging. In recent years, both theoretical and experimental work focusing on interacting Rydberg chains have made some exciting progress in this direction [42, 45, 49–51]. On the one hand, by adiabatically driving a Rydberg chain consisting of 51 neutral atoms through a possible period-3 ordered-to-disordered transition, researchers experimentally measured the corresponding Kibble-Zurek exponent μ in relation to other critical exponents via $\mu = \nu/(1 + z\nu)$ [15]. On the other hand, numerical studies [50] utilizing exact diagonalization and finite-size scaling methods have also extracted the dynamical critical exponent z in some parameter regimes. It can be observed that the critical exponent z varies continuously with the coupling strength (or equivalently, the blockade radius), recovering an exponent value similar to that of the \mathbb{Z}_3 chiral clock model. This behavior suggests that in addition to the three-state Potts criticality with $z = 1$, a direct continuous chiral phase transitions of $z \neq 1$ also occurs. Notably, independent evidence of non-conformal chiral transitions was later provided for longer Rydberg chains [42] and infinite chains [46], as well as a potential floating phase which is only theoretically predicted between the incommensurate disordered and commensurate period-3 ordered phases. All these studies expanded our understanding of the C-IC transition and motivate us to further work in this research direction.

This prompts us to revisit the period-3 ordered-to-disordered transition in the Rydberg chain from a different perspective, namely, the fidelity susceptibility, as an independent exploration of this exotic transition. For the same reasons explained in the previous section, we consider system size $L = 3n + 1$, ranging from $L = 49$ to 127, to stabilize the period-3 ordering in the system. We also note that the truncation strategy adopted in our simulations with respect to long-range interactions, which is

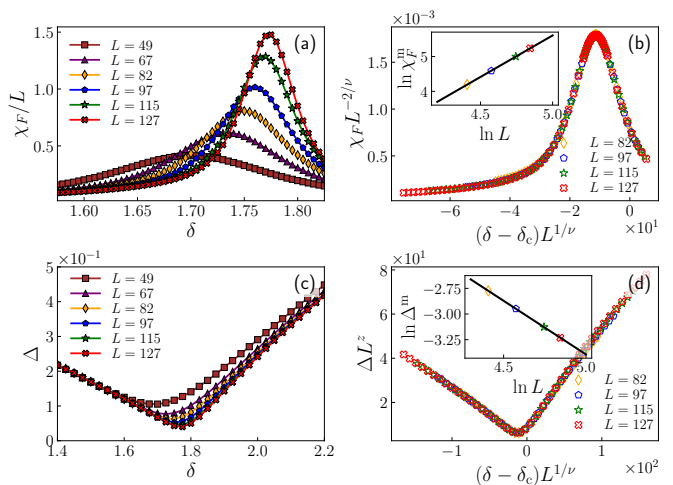


FIG. 4. Finite-size scaling analysis of fidelity susceptibility and energy gap for the period-3 ordered-to-disordered transition with $R_b = 2.3$. The fidelity susceptibility per site (a) and the energy gap (c) develop a sharp peak and a deep valley, respectively, near the phase transition point. A standard finite-size scaling method has been used to estimate the critical point $\delta_c = 1.808$, as well as the critical exponents $\nu = 0.838$ and $z = 1.044$.

mentioned in Sec. II. The DMRG-related parameters set here are the same as in the previous section.

We first investigate the case of $R_b = 2.3$ near the three-state Potts universality class by possessing critical exponents that is very close to the theoretical result for the universality class. Similar to the performance observed in the period-2 transition, it is evident from Fig. 4 that the fidelity susceptibility per site and the energy gap exhibit sharp peaks and deep valleys, respectively, around a certain detuning value signaling the occurrence of possible quantum phase transitions. After a standard finite-size scaling analysis following the same procedure described in Sec. III, the associated critical exponents can be numerically estimated as $\nu = 0.838$ and $z = 1.044$, which is consistent with the results for the three-state Potts universality class within numerical precision. In this sense, we can say that the case of $R_b = 2.3$ is very close to the exact three-state Potts critical point. It is worth noting that the precise Potts point can be located numerically with high precision by following the commensurate line $q = 2\pi/3$ in the disordered phase until the period-3 ordered phase is reached. More details can be found in references [42–45] for more details. Furthermore, we also examined the effect of the interaction cutoff adopted in our simulation on this $R_b = 2.3$ case. By further considering the fifth-nearest neighbor interaction $V(r = 5)$, we find the critical point exhibits a small shift of order 10^{-2} to the disordered region. This implies that the truncation $V(r > 4) = 0$ is a good approximation for actual long-range coupling and the critical point estimated here should be comparable to the one measured in actual experiments.

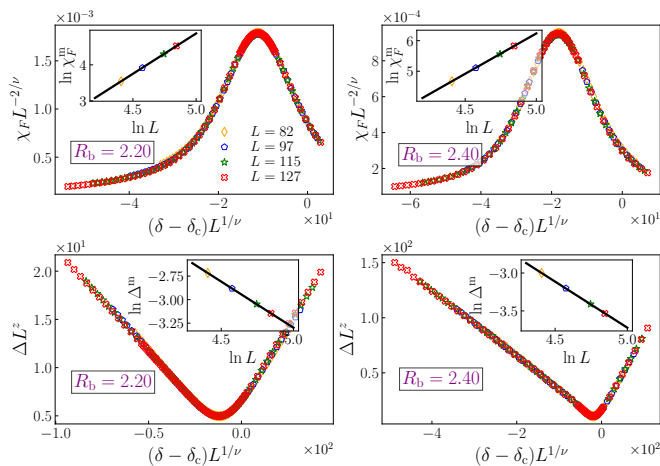


FIG. 5. Data collapse of the fidelity susceptibility and energy gap for blockade radius $R_b = 2.20$ and 2.40 , within the disordered to period-3 ordered transition regime based on the values of ν and z summarized in Table I. Data for different system sizes are denoted by different symbols: orange diamond for $L = 82$, blue pentagon for $L = 97$, green star for $L = 115$, and red cross for $L = 127$, as shown in the first plot (same for other plots). The value of the associated critical exponents is estimated, following the same logic obeyed in Sec. III, by the log-log plot of χ_F and Δ versus the chain length L at the pseudocritical point (see the insets of the plots).

To reveal the characteristics of direct chiral transitions, we next consider other blockade radius within the period-3 ordered-to-disordered transition regime. As shown in Figs. 5 and Appendix B, both the fidelity susceptibility and energy gap obey the conventional finite-size scaling law over a relatively wide blockade range. In Fig. 6 and Table I, we show the dependence of the exponents ν , z , and μ as a function of the Rydberg blockade radius R_b . The results show that these three critical exponents vary continuously with respect to the blockade radius in a monotonous manner, similar to the variation of the critical exponents of the chiral clock model reported in Ref. [50]. More specifically, the correlation length exponent ν decreases with increasing blockade radius, while the dynamical critical exponent z shows a steady increase with $\nu < \nu_{\text{potts}} = 5/6$ and $z > 1$ for $R_b \gtrsim 2.3$. However, for the other side $R_b < 2.3$, we find that the exponent z clearly converges to a certain value. Notably, the same trend was detected in small Rydberg chains with periodic boundary conditions [50]. Since our numerical values of ν should cross the exact point $\nu = \nu_{\text{potts}}$ at some blockade radius R_b^* accompanied with $z = 1$, we can expect a transition line of $z = 1$ to be terminated exactly at the three-state Potts point for $R_b \lesssim R_b^*$. This suggests that the phase transition differs from Potts universality for $\nu > 5/6$, but can still be described by CFTs. We note that the small difference between the estimated z and 1 can be explained by a potential finite-size effect. In addition, the value of the KZ exponent μ here can also serve as a useful guide for further KZ experiments.

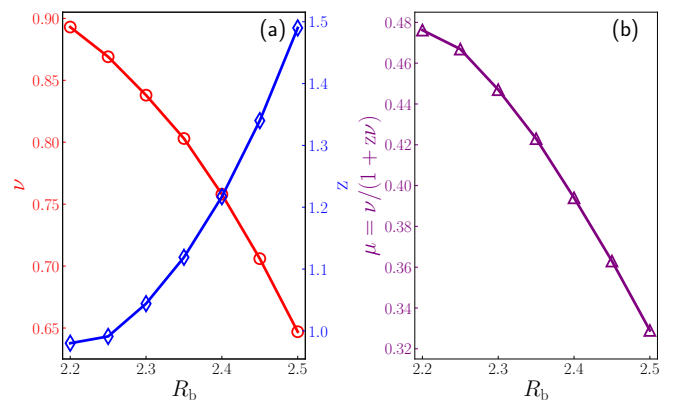


FIG. 6. (a) The correlation length exponent ν (red circles) and dynamical critical exponent z (blue diamonds) associated with the period-3 ordered-to-disordered transition for various blockade radius R_b . The values of ν and z are inferred from finite-size scaling analysis of χ_F and Δ with system sizes $L = 82$ up to 127 . (b) The Kibble-Zurek exponent μ (purple triangles) obtained from the estimated ν and z via the relation $\mu = \nu/(1 + z\nu)$ is shown as a function of the blockade radius.

TABLE I. Critical exponents of the period-2 and -3 ordered-to-disordered transitions realized by the Rydberg chain for different blockade radius R_b are summarized here for convenience. These exponents are extracted from finite-size scaling analysis of the fidelity susceptibility and energy gap.

R_b	δ_c	ν	z	μ
1.4	1.021(2)	1.034	0.9760	0.5146
1.6	1.210(2)	1.019	0.9847	0.5086
2.20	1.962(3)	0.893	0.980	0.4762
2.25	1.852(2)	0.869	0.991	0.4669
2.30	1.808(2)	0.838	1.044	0.4470
2.35	1.800(2)	0.803	1.119	0.4230
2.40	1.818(2)	0.758	1.217	0.394
2.45	1.856(2)	0.706	1.34	0.363
2.50	1.914(2)	0.647	1.49	0.329

To complete the exploration of the period-3 ordered-to-disordered transition and to examine the recently reported floating phase, in Fig. 7, we also investigate the case of $R_b = 2.6$, beyond the parameter regime explored in Fig. 5. Surprisingly, the fidelity susceptibility per site now clearly shows two nearby peaks as a function of detuning δ , implying that there may be another quantum phase different from the disordered or the period-3 ordered ones. Based on recent related works [42, 45, 49], we can expect this intermediate phase to be the so-called floating phase. Both of these susceptibility peaks become sharper with increasing chain length, and the floating phase is confined to a narrow parameter range, making its identification rather difficult. Unlike fitting the divergence of the correlation length in power or exponential form in Ref. [42], our results suggest another possible ap-

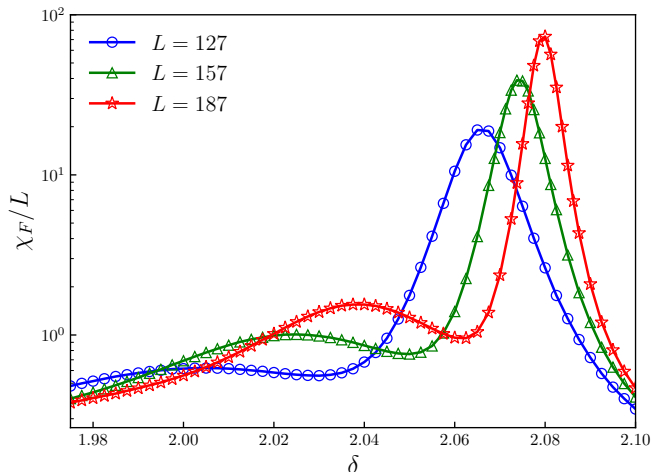


FIG. 7. Fidelity susceptibility per site χ_F/L as a function of δ for $R_b = 2.6$. χ_F/L shows two peaks as the system is driven from the disordered phase into the period-3 ordered phase indicating the possible existence of another floating phase between these two phases. The interval of these two peaks decreases as the system size is increased, which means the extent of the potential floating phase is very small, making its identification pretty hard.

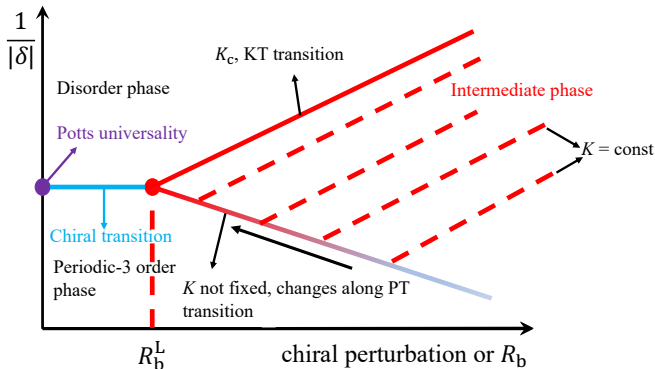


FIG. 8. Sketches of the possibilities for the explanation of our numerical results for the Rydberg chain. The Luttinger liquid parameter K changes along the PT transition and reaches the value of $K = K_c$ of the KT transition at the Lifshitz point R_b^L (red point). Beyond this point, the transition is non-conformal chiral transition until it reaches the standard three-state Potts critical point (purple point) when the chiral perturbation vanishes.

proach to determine the floating phase by extrapolating the pseudocritical point from χ_F to the thermodynamic limit.

In the following, we use the concept of Luttinger liquid to outline a general picture of the period-3 ordered-to-disordered transition realized in an interacting Rydberg chain. Since the Rydberg excitation number is not conserved in H_{Ryd} , the theoretical argument presented in Ref. [49] for the existence of a Lifshitz point, which draws a clear line between the chiral transition and the

floating phase at the $p = 3, 4$ C-IC transition, will also work in this case. We present a simple argument, summarized in Fig. 8, to explain our numerical results, based on the physical pictures provided in the reference [49]. Our simulation results are fundamentally consistent with the phase diagram mapped out in Refs. [42, 46]. A striking fact is that there are different types of domain walls associated with the commensurate period-3 ordering and the inequities between these domain walls lead to chiral perturbations. Furthermore, long-range interactions (parametrized by R_b) enhance this inequity, making the system “more chiral”. Thus, the gapless floating phase (described by the Luttinger liquid parameter K) effectively has “infinite” unequal domain walls, characterized by a varying wave vector q , and is located in the region of strong chiral perturbation (large R_b region). Since the Rydberg excitation number is not conserved, the Luttinger liquid parameter K is not fixed and will vary with the PT transition line as R_b decreases [49]. Moreover, the inequivalence between the domain walls is reduced, with the Luttinger liquid parameter $K < K_c$ for $R_b > R_b^L$, resulting in a stable intermediate floating phase. In addition, domain walls will proliferate as R_b decreases, and when $R_b = R_b^L$, the Luttinger liquid parameter would reach the value of $K = K_c$, at which point the floating phase begins to become unstable. Due to the limited chiral perturbation, this transition no longer occurs through the intermediate phase, which is far from the standard three-state Potts universality, thus opening the way for the chiral transition. Finally, the standard three-state Potts critical point is reached when the chiral perturbation disappears at a certain R_b value.

V. SUMMARY

In conclusion, we perform large-scale DMRG simulations to investigate the ground-state phase diagram of the Rydberg chains in certain parameter regions. Using fidelity susceptibility and energy gaps as diagnostics, we are able to efficiently locate quantum critical points between disordered and ordered phases of different density-wave orderings according to the Rydberg blockade radius R_b . For small R_b , the transition between the period-2 ordered and disordered phases belongs to the Ising universality class, characterized by $\nu = 1$ and $z = 1$, which is consistent with previous numerical and experimental results. For intermediate values of R_b ($2.3 \lesssim R_b \lesssim 2.5$), we found clear evidence of continuous chiral transition between the period-3 ordered and disordered phases with non-conformal critical points. In addition, the appearance of the double peaks shown in fidelity susceptibility also indicates the presence of an intermediate floating phase for large R_b . Our study clearly demonstrates the potential advantages of using the fidelity sensitivity concept to study this challenging critical phase transition and determine its parameter range. The study shows that fidelity susceptibility can be used as an effective

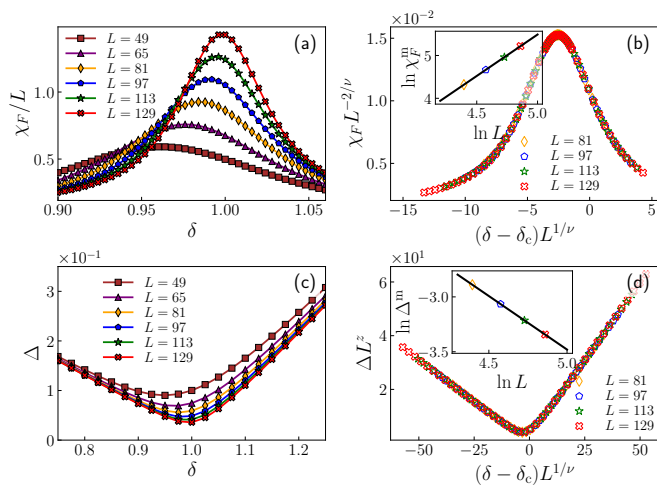


FIG. 9. Finite-size scaling analysis of fidelity susceptibility and energy gap for the period-2 ordered-to-disordered transition with a fixed blockade radius $R_b = 1.4$. The fidelity susceptibility per site χ_F/L (a) and the energy gap Δ (c) develop a sharp peak and a deep valley, respectively, near the quantum critical point. A standard finite-size scaling analysis has been applied to estimate the critical point $\delta_c = 1.021(2)$, as well as the critical exponents $\nu = 1.034$ and $z = 0.9760$.

probe to study general C-IC transitions and provides a quantum information perspective for understanding non-conformal quantum phase transitions in programmable quantum simulators.

ACKNOWLEDGMENTS

X.-J. Yu thank Zi-Xiang Li and Zhi Li for helpful discussions. Numerical simulations were carried out with the ITensor package [70]. We thank the computational resources provided by the TianHe-1A supercomputer, the High Performance Computing Platform of Peking University, China. X.-J.Y. and L.X. is supported by the National Natural Science Foundation of China under Grant No. 11935002, and the National Key R&D Program under Grant No. 2016YFA0300901. S.Y. and J.-B.X. is supported by the National Natural Science Foundation of China under Grant No. 11975198.

Appendix A: MORE EVIDENCE FOR ISING UNIVERSILITY CLASS: CRITICAL EXPONENTS FOR $R_b = 1.4$

In this appendix, we provide the finite-size scaling analysis of the fidelity susceptibility and energy gap with $R_b = 1.4$ to give more evidence that the period-2 ordered-to-disordered transition hosted by the Hamiltonian H_{Ryd} belongs to the $(1+1)$ D Ising universality class.

Using the same strategy adopted in Sec III, in Figs. 9(a) and (c), we can clearly observe the fidelity susceptibility per site and the energy gap develop, respectively, with an explicit peak and valley near a certain detuning indicating the transition from the disordered phase into the period-2 ordered phase. According to the finite-size scaling laws, the logarithms of χ_F and Δ are expected to exhibit linear dependence on $\ln L$; the corresponding least-square fittings are displayed in the insets of Fig. 9(b) and (d) from which we can extract the critical exponents $\nu = 1.034$ and $z = 0.9760$. With these estimated exponents, at last, we also achieve perfect curve collapses according to Eqs. (1) and (5) with a fine-tuned critical detuning $\delta_c = 1.021(2)$ as shown in Fig. 9(b) and (d).

Now we have investigated the phase transition at another blockade radius $R_b = 1.4$ which is within the period-2 ordered-to-disordered transition regime. The critical exponents acquired here also confirm the conclusion made in Sec III that the disorder to period-2 ordered-to-disordered transition in the programmable Rydberg chain belongs to the $(1+1)$ D Ising universality.

Appendix B: ADDITIONAL DATA COLLAPSE WITHIN THE PERIOD-3 ORDERED-TO-DISORDERED TRANSITION REGIME

In this appendix, we show additional data collapse of the fidelity susceptibility and energy gap for the blockade radius within the period-3 ordered-to-disordered transition regime.

Following the same procedure illustrated in the main text, the numerical values of the critical exponents ν and z are estimated by applying the finite-size scaling analysis. The fidelity susceptibility and energy gap for $R_b = 2.25, 2.35, 2.45, 2.50$ are shown in Fig. 10, which clearly shows that the critical exponents vary continuously with respect to the blockade radius in a monotonous manner.

-
- [1] S. Sachdev, *Quantum Phase Transitions*, 2nd ed. (Cambridge University Press, 2011).
 [2] S. L. Sondhi, S. M. Girvin, J. P. Carini, and D. Shahar, Continuous quantum phase transitions, *Rev. Mod. Phys.* **69**, 315 (1997).
 [3] P. A. Lee, N. Nagaosa, and X.-G. Wen, Doping a mott insulator:

- Physics of high-temperature superconductivity, *Rev. Mod. Phys.* **78**, 17 (2006).
 [4] H. L. Stormer, D. C. Tsui, and A. C. Gossard, The fractional quantum hall effect, *Rev. Mod. Phys.* **71**, S298 (1999).
 [5] Y. Zhou, K. Kanoda, and T.-K. Ng, Quantum spin liquid

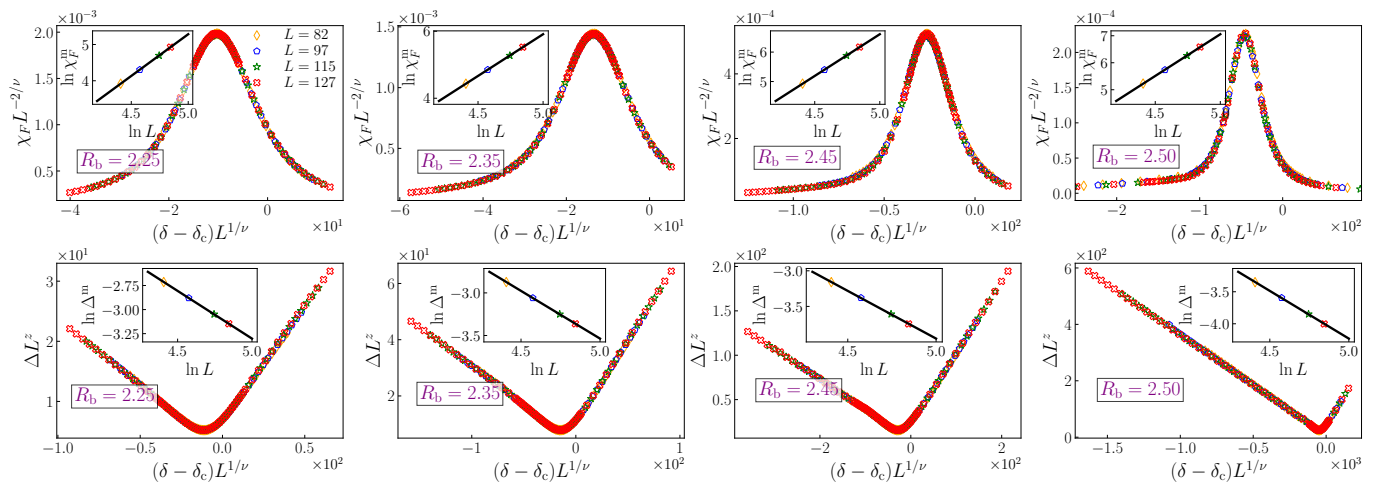


FIG. 10. Data collapse of the fidelity susceptibility and energy gap for other blockade radius R_b within the period-3 transition regime based on the values of ν and z collected in Table I. Different symbols are used to represent data for different system sizes: orange diamond for $L = 82$, blue pentagon for $L = 97$, green star for $L = 115$, and red cross for $L = 127$ (see the first plot). The critical exponents are extracted, following the same logic obeyed in Sec. III, from the log-log plot of χ_F and Δ versus the chain length L at the pseudocritical point (see the insets of the plots).

- states, *Rev. Mod. Phys.* **89**, 025003 (2017).
- [6] L. Savary and L. Balents, Quantum spin liquids: a review, *Reports on Progress in Physics* **80**, 016502 (2016).
- [7] F. Evers and A. D. Mirlin, Anderson transitions, *Rev. Mod. Phys.* **80**, 1355 (2008).
- [8] C. Xu, Unconventional quantum critical points, *International Journal of Modern Physics B* **26**, 1230007 (2012).
- [9] Z.-X. Guo, X.-J. Yu, X.-D. Hu, and Z. Li, Emergent phase transitions in a cluster ising model with dissipation, *Phys. Rev. A* **105**, 053311 (2022).
- [10] X.-J. Yu, P.-L. Zhao, S.-K. Jian, and Z. Pan, Emergent space-time supersymmetry at disordered quantum critical points, *Phys. Rev. B* **105**, 205140 (2022).
- [11] X.-J. Yu, R.-Z. Huang, H.-H. Song, L. Xu, C. Ding, and L. Zhang, Conformal boundary conditions of symmetry-enriched quantum critical spin chains, *arXiv preprint arXiv:2111.10945* (2021).
- [12] J. Cardy, *Scaling and Renormalization in Statistical Physics*, Cambridge Lecture Notes in Physics (Cambridge University Press, 1996).
- [13] P. Francesco, P. Mathieu, and D. Sénéchal, *Conformal field theory* (Springer Science & Business Media, 2012).
- [14] P. Ginsparg, Applied conformal field theory, *arXiv preprint hep-th/9108028* (1988).
- [15] A. Keesling, A. Omran, H. Levine, H. Bernien, H. Pichler, S. Choi, R. Samajdar, S. Schwartz, P. Silvi, S. Sachdev, *et al.*, Quantum kibble-zurek mechanism and critical dynamics on a programmable rydberg simulator, *Nature* **568**, 207 (2019).
- [16] H. Bernien, S. Schwartz, A. Keesling, H. Levine, A. Omran, H. Pichler, S. Choi, A. S. Zibrov, M. Endres, M. Greiner, *et al.*, Probing many-body dynamics on a 51-atom quantum simulator, *Nature* **551**, 579 (2017).
- [17] S. Ebadi, T. T. Wang, H. Levine, A. Keesling, G. Semeghini, A. Omran, D. Bluvstein, R. Samajdar, H. Pichler, W. W. Ho, *et al.*, Quantum phases of matter on a 256-atom programmable quantum simulator, *Nature* **595**, 227 (2021).
- [18] A. Browaeys and T. Lahaye, Many-body physics with individually controlled rydberg atoms, *Nature Physics* **16**, 132 (2020).
- [19] R. Verresen, M. D. Lukin, and A. Vishwanath, Prediction of toric code topological order from rydberg blockade, *Phys. Rev. X* **11**, 031005 (2021).
- [20] G. Semeghini, H. Levine, A. Keesling, S. Ebadi, T. T. Wang, D. Bluvstein, R. Verresen, H. Pichler, M. Kalinowski, R. Samajdar, *et al.*, Probing topological spin liquids on a programmable quantum simulator, *Science* **374**, 1242 (2021).
- [21] G. Giudici, M. D. Lukin, and H. Pichler, Dynamical preparation of quantum spin liquids in rydberg atom arrays, *arXiv preprint arXiv:2201.04034* (2022).
- [22] Z. Yan, R. Samajdar, Y.-C. Wang, S. Sachdev, and Z. Y. Meng, Triangular lattice quantum dimer model with variable dimer density, *arXiv preprint arXiv:2202.11100* (2022).
- [23] K. Slagle, Y. Liu, D. Aasen, H. Pichler, R. S. Mong, X. Chen, M. Endres, and J. Alicea, Quantum spin liquids bootstrapped from ising criticality in rydberg arrays, *arXiv preprint arXiv:2204.00013* (2022).
- [24] R. Samajdar, D. Joshi, Y. Teng, and S. Sachdev, Emergent $z = 2$ gauge theories and topological excitations in rydberg quantum simulators, *Bulletin of the American Physical Society* (2022).
- [25] G. Giudice, F. M. Surace, H. Pichler, and G. Giudici, Trimer states with backslash \mathbb{Z}_3 topological order in rydberg atom arrays, *arXiv preprint arXiv:2205.10387* (2022).
- [26] R. Verresen and A. Vishwanath, Unifying kitaev magnets, kagome dimer models and ruby rydberg spin liquids (2022).
- [27] G.-Q. An, T. Wang, and X.-F. Zhang, Quantum phase transition of the two-dimensional rydberg atom array in an optical cavity, *arXiv preprint arXiv:2204.08800* (2022).
- [28] M. J. O'Rourke and G. K. Chan, Entanglement in the

- quantum phases of an unfrustrated rydberg atom array, [arXiv preprint arXiv:2201.03189](#) (2022).
- [29] M. Kalinowski, R. Samajdar, R. G. Melko, M. D. Lukin, S. Sachdev, and S. Choi, Bulk and boundary quantum phase transitions in a square rydberg atom array, *Phys. Rev. B* **105**, 174417 (2022).
- [30] R. Samajdar, W. W. Ho, H. Pichler, M. D. Lukin, and S. Sachdev, Quantum phases of rydberg atoms on a kagome lattice, *Proceedings of the National Academy of Sciences* **118** (2021).
- [31] R. Samajdar, W. W. Ho, H. Pichler, M. D. Lukin, and S. Sachdev, Complex density wave orders and quantum phase transitions in a model of square-lattice rydberg atom arrays, *Phys. Rev. Lett.* **124**, 103601 (2020).
- [32] K. Slagle, D. Aasen, H. Pichler, R. S. K. Mong, P. Fendley, X. Chen, M. Endres, and J. Alicea, Microscopic characterization of ising conformal field theory in rydberg chains, *Phys. Rev. B* **104**, 235109 (2021).
- [33] A. Chandran, F. J. Burnell, and S. L. Sondhi, Absence of fibonacci anyons in rydberg chains, *Phys. Rev. B* **101**, 075104 (2020).
- [34] N. Chepiga and F. Mila, Kibble-zurek exponent and chiral transition of the period-4 phase of rydberg chains, *Nature Communications* **12**, 1 (2021).
- [35] R.-Z. Huang and S. Yin, Nonequilibrium critical dynamics in the quantum chiral clock model, *Phys. Rev. B* **99**, 184104 (2019).
- [36] C. J. Turner, A. A. Michailidis, D. A. Abanin, M. Serbyn, and Z. Papić, Weak ergodicity breaking from quantum many-body scars, *Nature Physics* **14**, 745 (2018).
- [37] M. Serbyn, D. A. Abanin, and Z. Papić, Quantum many-body scars and weak breaking of ergodicity, *Nature Physics* **17**, 675 (2021).
- [38] S. Ostlund, Incommensurate and commensurate phases in asymmetric clock models, *Phys. Rev. B* **24**, 398 (1981).
- [39] D. A. Huse, Simple three-state model with infinitely many phases, *Phys. Rev. B* **24**, 5180 (1981).
- [40] D. A. Huse and M. E. Fisher, Domain walls and the melting of commensurate surface phases, *Phys. Rev. Lett.* **49**, 793 (1982).
- [41] D. A. Huse and M. E. Fisher, Commensurate melting, domain walls, and dislocations, *Phys. Rev. B* **29**, 239 (1984).
- [42] I. A. Maceira, N. Chepiga, and F. Mila, [Conformal and chiral phase transitions in rydberg chains](#) (2022).
- [43] S. Nyckees, J. Colbois, and F. Mila, Identifying the huse-fisher universality class of the three-state chiral potts model, *Nuclear Physics B* **965**, 115365 (2021).
- [44] S. Nyckees and F. Mila, Commensurate-incommensurate transition in the chiral ashkin-teller model, *Phys. Rev. Research* **4**, 013093 (2022).
- [45] N. Chepiga and F. Mila, Floating phase versus chiral transition in a 1d hard-boson model, *Phys. Rev. Lett.* **122**, 017205 (2019).
- [46] M. Rader and A. M. Läuchli, Floating phases in one-dimensional rydberg ising chains, [arXiv preprint arXiv:1908.02068](#) (2019).
- [47] P. Fendley, K. Sengupta, and S. Sachdev, Competing density-wave orders in a one-dimensional hard-boson model, *Phys. Rev. B* **69**, 075106 (2004).
- [48] S. Sachdev, K. Sengupta, and S. M. Girvin, Mott insulators in strong electric fields, *Phys. Rev. B* **66**, 075128 (2002).
- [49] N. Chepiga and F. Mila, Lifshitz point at commensurate melting of chains of rydberg atoms, *Phys. Rev. Research* **3**, 023049 (2021).
- [50] R. Samajdar, S. Choi, H. Pichler, M. D. Lukin, and S. Sachdev, Numerical study of the chiral \mathbb{Z}_3 quantum phase transition in one spatial dimension, *Phys. Rev. A* **98**, 023614 (2018).
- [51] S. Whitsitt, R. Samajdar, and S. Sachdev, Quantum field theory for the chiral clock transition in one spatial dimension, *Phys. Rev. B* **98**, 205118 (2018).
- [52] S.-J. Gu, Fidelity approach to quantum phase transitions, *International Journal of Modern Physics B* **24**, 4371 (2010).
- [53] A. F. Albuquerque, F. Alet, C. Sire, and S. Capponi, Quantum critical scaling of fidelity susceptibility, *Phys. Rev. B* **81**, 064418 (2010).
- [54] Z. Zhu, G. Sun, W.-L. You, and D.-N. Shi, Fidelity and criticality of a quantum ising chain with long-range interactions, *Phys. Rev. A* **98**, 023607 (2018).
- [55] G. Sun, Fidelity susceptibility study of quantum long-range antiferromagnetic ising chain, *Phys. Rev. A* **96**, 043621 (2017).
- [56] G. Sun, A. K. Kolezhuk, and T. Vekua, Fidelity at berezinskii-kosterlitz-thouless quantum phase transitions, *Phys. Rev. B* **91**, 014418 (2015).
- [57] B.-B. Wei, Fidelity susceptibility in one-dimensional disordered lattice models, *Phys. Rev. A* **99**, 042117 (2019).
- [58] T. Lv, T.-C. Yi, L. Li, G. Sun, and W.-L. You, Quantum criticality and universality in the p -wave-paired aubry-andré-harper model, *Phys. Rev. A* **105**, 013315 (2022).
- [59] G. Sun, B.-B. Wei, and S.-P. Kou, Fidelity as a probe for a deconfined quantum critical point, *Phys. Rev. B* **100**, 064427 (2019).
- [60] G. Sun, J.-C. Tang, and S.-P. Kou, Biorthogonal quantum criticality in non-hermitian many-body systems, *Frontiers of Physics* **17**, 1 (2022).
- [61] Y.-C. Tzeng, C.-Y. Ju, G.-Y. Chen, and W.-M. Huang, Hunting for the non-hermitian exceptional points with fidelity susceptibility, *Phys. Rev. Research* **3**, 013015 (2021).
- [62] Y.-T. Tu, I. Jang, P.-Y. Chang, and Y.-C. Tzeng, General properties of fidelity in non-hermitian quantum systems with pt symmetry, [arXiv preprint arXiv:2203.01834](#) (2022).
- [63] S.-J. Gu and W. C. Yu, Spectral function and fidelity susceptibility in quantum critical phenomena, *EPL (Europhysics Letters)* **108**, 20002 (2014).
- [64] S. R. White, Density matrix formulation for quantum renormalization groups, *Phys. Rev. Lett.* **69**, 2863 (1992).
- [65] U. Schollwöck, The density-matrix renormalization group in the age of matrix product states, *Annals of Physics* **326**, 96 (2011), january 2011 Special Issue.
- [66] D. Perez-Garcia, F. Verstraete, M. M. Wolf, and J. I. Cirac, Matrix product state representations, [arXiv preprint quant-ph/0608197](#) (2006).
- [67] S. Chen, L. Wang, Y. Hao, and Y. Wang, Intrinsic relation between ground-state fidelity and the characterization of a quantum phase transition, *Phys. Rev. A* **77**, 032111 (2008).
- [68] W.-L. You, Y.-W. Li, and S.-J. Gu, Fidelity, dynamic structure factor, and susceptibility in critical phenomena, *Phys. Rev. E* **76**, 022101 (2007).
- [69] S.-J. Gu, H.-M. Kwok, W.-Q. Ning, and H.-Q. Lin, Fidelity susceptibility, scaling, and universality in quantum critical phenomena, *Phys. Rev. B* **77**, 245109 (2008).

- [70] M. Fishman, S. R. White, and E. M. Stoudenmire, The itensor software library for tensor network calculations, [arXiv preprint arXiv:2007.14822](#) **28** (2020).